

# Derivation of Buckling Knockdown Factors Using The Equivalent Model for Isogrid-Stiffened Cylinders

Han-Il Kim<sup>1\*</sup>, Chang-Hoon Sim<sup>2\*</sup>, Jae-Sang Park<sup>3\*</sup>, Keejoo Lee<sup>4§</sup>, Joon-Tae Yoo<sup>5§</sup>, and Young-Ha Yoon<sup>6§</sup>

\*Chungnam National University, Daejeon, Korea

<sup>1</sup>hikim11@cnu.ac.kr, <sup>2</sup>sch91@cnu.ac.kr, <sup>3</sup>aerotor@cnu.ac.kr

<sup>§</sup>Korea Aerospace Research Institute, Daejeon, Korea

<sup>4</sup>klee@kari.re.kr, <sup>5</sup>jtyoo@kari.re.kr, <sup>6</sup>yhyoon@kari.re.kr

## Abstract

This study attempts to derive numerically the shell Knockdown factors of isogrid-stiffened cylinders under axial compressive loads. Various shell thickness ratios are considered for the isogrid-stiffened cylinders. Two different modeling techniques such as the detailed modeling with numerous stiffeners and the equivalent modeling without modeling of stiffeners are applied for the present work. The single perturbation load approach (SPLA) is used to represent the geometrical initial imperfection of a cylinder. Postbuckling analyses with the displacement control method are conducted to derive numerically the shell Knockdown factors of isogrid-stiffened cylinders. The global buckling loads and shell Knockdown factors using the equivalent model are excellently compared with the results with the detailed model although the computation time using the equivalent model is 13 to 16% of that with the detailed model. The present Knockdown factor function in terms of the shell thickness ratio for the isogrid-stiffened cylinder is much higher than NASA's Knockdown factor function; therefore, it is believed that the present Knockdown factor function can facilitate in developing lightweight launch vehicle structures using the isogrid-stiffened cylinder.

## 1. Introduction

The thin cylindrical structure is the most important structural element for space launch vehicles. However it is very vulnerable to various loads, particularly axial compressive loads, on the launch pad and during the flight. Therefore, thin cylinders usually use many stiffeners in both the axial and circumferential directions of a cylinder to improve the stiffness and strength. The stiffeners are generally used in a grid form such as the orthogrid and isogrid-stiffened systems (Figure 1). The isogrid-stiffened system uses a lattice of intersecting ribs forming an array of equilateral triangles as given in Figure 1(b), and it provides the isotropic behaviors of a stiffened structure while improving the buckling load of a cylindrical structure, therefore, the isogrid-stiffened cylinder is frequently used for the propellant tanks and inter-tanks of a space launch vehicle.

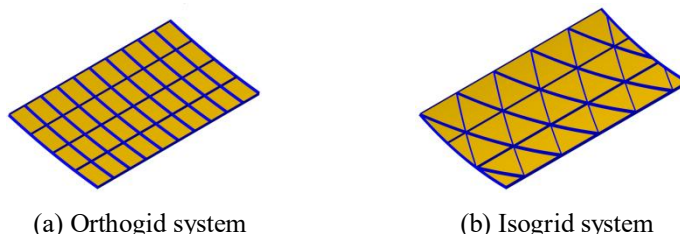


Figure 1: Grid-stiffened systems.

The buckling load is an essential factor in the structural design of the launch vehicle. However, the measured buckling load is usually lower than the calculated value from the linear buckling analysis. Among various reasons for this discrepancy between the linear buckling analysis and test, the geometrical initial imperfection of a thin shell structure is considered as the most important reason. The buckling Knockdown factor is introduced to reduce appropriately the predicted buckling load using a linear analysis. The Knockdown factor is defined as a ratio between the global buckling

loads of a thin shell structure with and without the initial imperfection. NASA provided the lower bound of Knockdown factors of the cylindrical structure (Figure 2, [1]) using the measured data through the buckling tests from 1930s to 1960s.

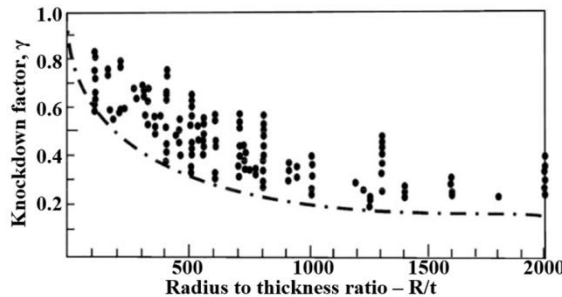


Figure 2: NASA's lower bound of Knockdown factors [1].

Therefore, this buckling design criteria (NASA's the lower bound of Knockdown factors) cannot consider the modern manufacturing technologies and advanced materials for launch vehicle structures, as a result, the launch vehicle structure is conservatively designed, that is, over-weight designed. Thus, two recent research projects, NASA's SBKF (Shell Buckling Knockdown Factor) project [2] and EU's DESICOS (New Robust DESign Guideline for Imperfection Sensitive Composite Launcher Structure) project [3] derived newly the Knockdown factor using extensive numerical analyses along with buckling tests for design of the lightweight launch vehicle structures. In the SBKF project, the metallic orthogrid-stiffened cylinders were considered and the shell Knockdown factors were derived numerically from the postbuckling analyses [4-6]. The SBKF project showed that the advanced numerical analysis can provide accurately the Knockdown factor of the orthogrid-stiffened cylinder and the derived shell Knockdown factor can give the lightweight design the space launch vehicle structures [4-6]. For the DESICOS project, composite cylinders without stiffeners were considered to derive the Knockdown factor numerically, and the numerical studies [7-9] showed that the derived Knockdown factors are higher than NASA's buckling design criteria. Along with these works [4-9], the extensive postbuckling numerical analyses [10] were conducted for various cylinders such as unstiffened isotropic/composite cylinders and orthogrid-stiffened cylinders, and the obtained results were compared with the previous Knockdown factors. In addition, the nonlinear postbuckling analyses were conducted in depth for the traditional orthogrid-stiffened and hybrid-grid stiffened cylinders, and the Knockdown factors were numerically derived using the calculated buckling loads with and without the geometrical initial imperfection [11]. In the work, the numerical analysis based buckling design provided higher Knockdown factors as compared to the NASA's Knockdown factors [1], and the hybrid-grid stiffened cylinder is more efficient than the traditional orthogrid-stiffened cylinder from the perspective of buckling design along with considering the structural weight.

As previously described, the thin shell structure with the isogrid-stiffened system shows an isotropic behavior structurally, thus the isogrid-stiffened cylinder can be modeled using the equivalent model without the detailed modeling of numerous stiffeners [12-14]. This equivalent model for the isogrid-stiffened structure provides efficient and appropriately precise computations for the overall structural behaviors such as the global buckling. Although the isogrid-stiffened cylindrical structures are widely used for the space launch vehicles, there have been limited works for the postbuckling analyses and numerical derivation of shell Knockdown factors considering various shell thickness ratios (ratio of radius to thickness). However the Knockdown factors of the isogrid-stiffened cylinder considering different shell thickness ratios are required for buckling design of space launch vehicles with various dimensions (from a small launch vehicle to a large one).

Therefore this study aims to derive numerically the Knockdown factors of isogrid-stiffened cylinders considering various shell thickness ratios ( $R/t_{eff}=100, 200, 300$ , and  $441$ ). For the finite element model of isogrid-stiffened cylinders, the detailed model considering numerous stiffeners and the equivalent model without the modeling of stiffeners both are used. A commercial nonlinear finite element analysis program, ABAQUS (version 6.16), is used for the present postbuckling analyses of isogrid-stiffened cylinders with and without the initial imperfection. The geometrical initial imperfection of a cylinder is modeled using the SPLA (Single Perturbation Load Approach [15-18]) which represents the best realistic and worst initial imperfection of shell structures. In this study, the slightly modified modeling technique for the SPLA [19, 20] to the original modeling technique [21] is used. The postbuckling analyses and Knockdown factors of isogrid-stiffened cylinders using the detailed and equivalent models are compared to each other for various shell thickness ratios to validate the equivalent modeling techniques for the isogrid-stiffened cylinder. Finally, the Knockdown factor function in terms of the shell thickness ratio is expressed using the numerically derived Knockdown factors. The derived Knockdown factor function for the isogrid-stiffened cylinder is compared to the

NASA's Knockdown factor function in order to investigate that the present buckling design criteria can provide lighter weight design of space launch vehicles.

## 2. Analytical method

### 2.1 Equivalent modeling

Since the isogrid-stiffened system shows the unique characteristics of isotropic behaviors, the isogrid-stiffened structure can be modeled as an equivalent and simple model without detailed modeling of numerous stiffeners. The following equations (1) to (6) derive the equivalent elastic modulus ( $E^*$ ) and equivalent thickness ( $t^*$ ) of the equivalent and simple cylinder model to the isogrid-stiffened cylinder [12].

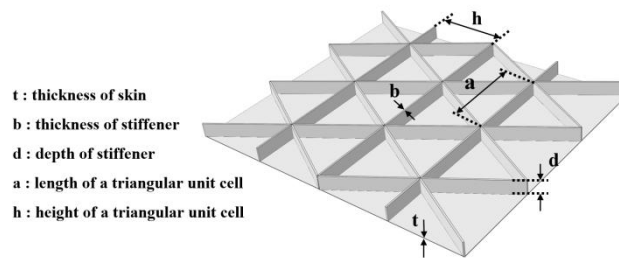


Figure 3: Schematic diagram of isogrid-stiffened system.

The height ( $h$ ) of a triangular unit cell given in Figure 3 for the isogrid-stiffened system is defined using Eq. (1) as

$$h = (\sqrt{3}/2)a \quad (1)$$

where  $a$  is the length of a triangular unit cell. In addition,  $\alpha$  is defined as

$$\alpha = bd / th \quad (2)$$

where  $b$  and  $d$  are the thickness and length of a stiffener, respectively. Furthermore, the skin thickness of the isogrid-stiffened cylinder is denoted as  $t$ . Eq. (3) shows the relation between  $d$  and  $t$  as

$$\delta = d / t \quad (3)$$

Using  $\alpha$  and  $\delta$ , Equation (4) can be defined as

$$\beta = [3\alpha(1+\delta)^2 + (1+\alpha)(1+\alpha\delta^2)]^{1/2} \quad (4)$$

Finally, the equivalent elastic modulus ( $E^*$ ) is calculated using  $\alpha$  and  $\beta$ .

$$E^* = E_0((1+\alpha)^2 / \beta) \quad (5)$$

$$t^* = t(\beta / 1 + \alpha) \quad (6)$$

where  $E_0$  is the elastic modulus of a detailed model. When the equivalent elastic modulus ( $E^*$ ) and thickness ( $t^*$ ) are used for modeling, the equivalent model for an isogrid-stiffened cylinder can be obtained without modeling of numerous stiffeners. The equivalent thickness ( $t^*$ ) defined in Eq. (6) is equal to the effective thickness ( $t_{eff}$ ) of the isogrid-stiffened cylinder. The equivalent model can save computation time and effort of finite element modeling appropriately as compared to the detailed model with modeling of stiffeners.

## 2.2 Modeling of isogrid-stiffened cylinders with various shell thickness ratios

There are a lot of cases to change the shell thickness ratio ( $R/t_{\text{eff}}$ ) of the isogrid-stiffened cylinder. Therefore, in this work, the radius ( $R$ ) of a cylinder is changed but the effective thickness of a cylinder ( $t_{\text{eff}}$ ) is maintained as the value of the baseline isogrid-stiffened cylinder model summarized in Table 1 and Figure 3 to reduce the number of cases to vary the shell thickness ratio.

Table 1: Properties of the baseline stiffened cylinder ( $R/t_{\text{eff}}=441$ , [22]).

| Property                              | Value      |
|---------------------------------------|------------|
| Thickness ratio, $R/t_{\text{eff}}$   | 441        |
| Radius, $R$                           | 2.250 m    |
| Length, $L$                           | 2.200 m    |
| Length of resin ring, $L_r$           | 0.083 m    |
| Length of a triangular unit cell, $a$ | 0.415 m    |
| Height of a triangular unit cell, $h$ | 0.360 m    |
| Thickness of stiffener, $b$           | 0.004 m    |
| Thickness of skin, $t$                | 0.004 m    |
| Depth of stiffener, $d$               | 0.008 m    |
| Angle of stiffener, $\theta$          | $60^\circ$ |
| Elastic modulus, $E_0$                | 73.1 GPa   |
| Poisson's ratio, $\nu$                | 0.33       |

When the value of  $d$  given in Eq. (3) is fixed as the baseline value, the effective thickness ( $t_{\text{eff}}$ ) can be also fixed. In addition, the values of  $R/L$ ,  $L/a$ , and  $b/h$  are maintained as their baseline values, respectively. The modeling procedure for the geometric properties of isogrid-stiffened cylinders with various shell thickness ratios is described as follows. First, the value of  $\delta$  is fixed as the baseline value in Table 1 as given in Eq. (7).

$$\delta_{\text{baseline}} = (d / t)_{\text{baseline}} \quad (7)$$

Second, using the given shell thickness ratio ( $R/t_{\text{eff}})_{\text{present}}$  and the baseline value of the effective thickness ( $t_{\text{eff}}$ ) in Table 1, the radius ( $R_{\text{present}}$ ) of a cylinder can be determined as

$$R_{\text{present}} = t_{\text{eff}} (R / t_{\text{eff}})_{\text{baseline}} \quad (8)$$

Third, since the slenderness ratio ( $R/L$ ) has a significant influence on the buckling characteristics of a cylinder, the value of  $R/L$  is maintained as the baseline value in Table 1. Therefore, along with the radius of a cylinder previously determined in Eq. (8),  $R_{\text{present}}$ , the length of a cylinder is designed as

$$L_{\text{present}} = R_{\text{present}} (R / L)_{\text{baseline}} \quad (9)$$

Fourth, the length of a triangular unit cell is determined using Eq. (10) in order to maintain the value of ( $L/a$ ) as the baseline value as

$$a_{\text{present}} = L_{\text{present}} (L / a)_{\text{baseline}} \quad (10)$$

Fifth, for the given shell thickness ratio, the height of a triangular unit cell (in Figure 3) is obtained using previously given in Eq. (10) as

$$h_{\text{present}} = (\sqrt{3} / 2) a_{\text{present}} \quad (11)$$

where Eq. (11) is the same as Eq. (1).

Finally, the thickness of a stiffener for the given shell thickness ratio can be designed to maintain the baseline value in Table 1 as

$$b_{\text{present}} = h_{\text{present}} (b / h)_{\text{baseline}} \quad (12)$$

After the design of a detailed model described above is completed for the given shell thickness ratio, the equivalent elastic modulus and thickness can be determined using Eqs. (5) and (6) to obtain the equivalent model of an isogrid-stiffened cylinder. In addition, the radius and length of an equivalent model are the same as those of the detailed model ( $R_{\text{present}}$  and  $L_{\text{present}}$ , respectively).

### 2.3 Isogrid-stiffened cylinder models

The baseline model of an isogrid-stiffened cylinder (the shell thickness ratio of  $R/t_{\text{eff}}=441$ ) is given in the previous Table 1 and Figure 4 [22]. The material properties (2024 Aluminum alloy) are the elastic modulus ( $E_0$ ) of 73.1 GPa and Poisson's ratio of 0.33. The cylinder consists of four stiffened panels and unstiffened straps (weld lands) between panels shown in Figure 4. For the boundary conditions of a cylinder, all the degree of freedoms at the bottom edge are constrained, but all the degree of freedoms except the translational degree of freedom in the z-direction are constrained at the top edge in Figure 4. Because of the lack of detailed modeling information given in Ref. [22], the thickness of a strap is assumed appropriately in the present detailed model. It is noteworthy that the equivalent modeling technique is applied only to the grid stiffened panel, not to the straps. Thus, the thickness of the strap for the equivalent model is equal to the thickness of the strap for the detailed model. When the modeling technique considering for various shell thickness ratios described in the previous section is applied, the detailed properties of isogrid-stiffened cylinders using the detailed and equivalent models are summarized in Tables 2 and 3.

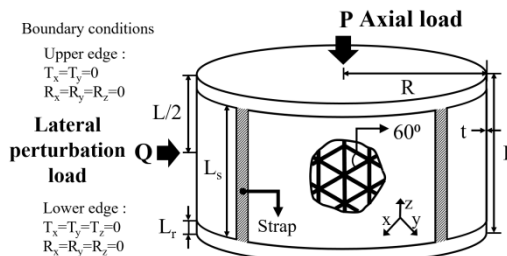


Figure 4: Schematic diagram of the isogrid-stiffened cylinder.

Table 2: Properties of the detailed models for isogrid-stiffened cylinders with various shell thickness ratios.

| Thickness ratio, $R/t_{\text{eff}}$   | 100      | 200      | 300      | 441      |
|---------------------------------------|----------|----------|----------|----------|
| Radius, $R$                           | 0.510 m  | 1.020 m  | 1.530 m  | 2.250 m  |
| Length, $L$                           | 0.500 m  | 1.000 m  | 1.500 m  | 2.200 m  |
| Length of resin ring, $L_r$           | 0.019 m  | 0.038 m  | 0.056 m  | 0.083 m  |
| Length of a triangular unit cell, $a$ | 0.094 m  | 0.188 m  | 0.282 m  | 0.415 m  |
| Height of a triangular unit cell, $h$ | 0.082 m  | 0.136 m  | 0.244 m  | 0.360 m  |
| Thickness of stiffener, $b$           | 0.0009 m | 0.0018 m | 0.0027 m | 0.0040 m |
| Thickness of skin, $t$                |          | 0.004 m  |          |          |
| Depth of stiffener, $d$               |          | 0.008 m  |          |          |
| Angle of stiffener, $\theta$          |          | 60°      |          |          |
| Elastic modulus, $E_0$                |          | 73.1 GPa |          |          |
| Poisson's ratio, $\nu$                |          | 0.33     |          |          |

Table 3: Properties of the equivalent models for isogrid-stiffened cylinders with various shell thickness ratios.

| Thickness ratio, $R/t_{\text{eff}}$ | 100     | 200       | 300     | 441     |
|-------------------------------------|---------|-----------|---------|---------|
| Radius, $R$                         | 0.510 m | 1.020 m   | 1.530 m | 2.250 m |
| Length, $L$                         | 0.500 m | 1.000 m   | 1.500 m | 2.200 m |
| Length of resin ring, $L_r$         | 0.019 m | 0.038 m   | 0.056 m | 0.083 m |
| Equivalent thickness, $t^*$         |         | 0.0051 m  |         |         |
| Equivalent elastic modulus, $E^*$   |         | 58.35 GPa |         |         |
| Poisson's ratio, $\nu$              |         | 0.33      |         |         |

## 2.4 Techniques for finite element modelling and analyses of isogrid-stiffened cylinders

A nonlinear finite element analysis program, ABAQUS, is used for the present postbuckling analyses of isogrid-stiffened cylinders under axial compressive loads. For the detailed modeling (Figure 5(a)), the skin structures for the grid-stiffened region are modeled using 3-node shell elements, however the stiffener and straps are modeled with 4-node shell elements; however, 4-node shell elements only are used for the equivalent modeling of the isogrid-stiffened cylinder (Figure 5(b)). The number of finite elements for the equivalent model is determined by the convergence test for the global buckling load, Table 4 shows the number of finite elements for the present modeling of isogrid-stiffened cylinders considering various shell thickness ratios. As seen in the table, the equivalent model use much less finite elements for finite element modeling than the detailed model, since the equivalent model does not model the stiffeners and represents the isogrid-stiffened cylinder as a simple cylinders without stiffeners.

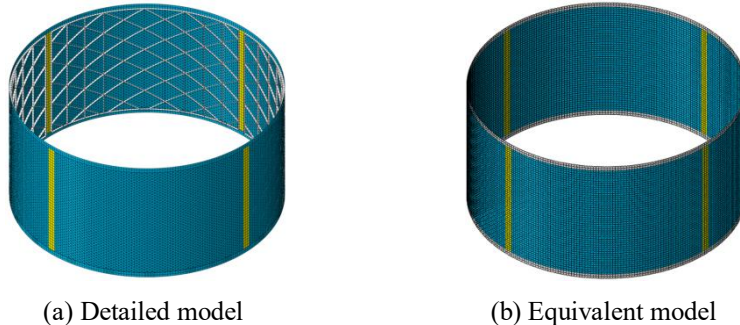


Figure 5: ABAQUS finite element models for the isogrid-stiffened cylinder.

Table 4: Number of finite elements of the isogrid-stiffened cylinders with various shell thickness ratios.

| Thickness ratio, $R/t_{eff}$ | 100    | 200    | 300    | 441    |
|------------------------------|--------|--------|--------|--------|
| Detailed model               | 33,228 | 33,288 | 33,128 | 33,128 |
| Equivalent model             |        |        | 17,064 |        |

## 2.5 Analysis techniques

The SPLA is considered as the best method to represent the geometrical initial imperfection of thin shell structures since it may represent the realistic and worst geometric imperfection of cylindrical structures [15-18]. Therefore, the SPLA is used to represent the geometrical initial imperfection of both the detailed and equivalent models for the present isogrid-stiffened cylinders. The SPLA is represented using the following three-step process [19] that is slightly different from the original modelling [21] as follows. First, an assumed perturbation load ( $Q$ ) in the radial direction is applied to the middle of an isogrid-stiffened cylinder (Figure 6(a)). For the detailed model of an isogrid-stiffened cylinder, the radial perturbation load is applied to the point of an intersection between the axial stiffener of a grid panel and middle line of a cylinder as shown in Figure 6(b); however, the application point of a radial perturbation load for the equivalent model is considered as the same point for the detailed model.

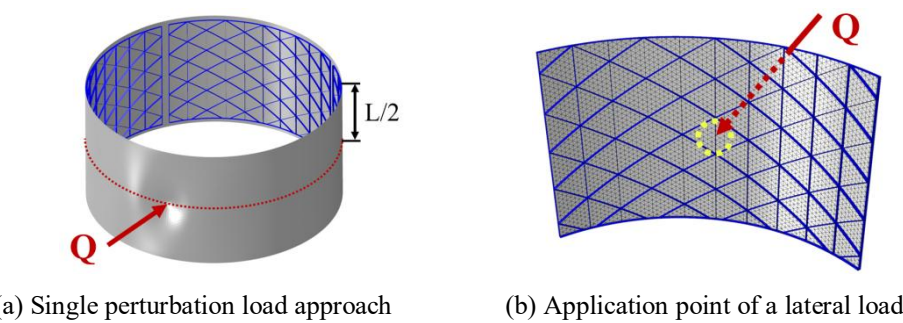


Figure 6: Single perturbation load approach (SPLA).

A nonlinear static analysis using ABAQUS is conducted for the isogrid-stiffened cylinder under the prescribed radial perturbation load in this step. Second, the deformed configuration of a cylinder is imposed to the perfect cylinder by modifying the nodal coordinates of the cylinder's finite element model. This modeling can represent a cylinder with a geometrical initial imperfection in a stress-free state, which is a realistic modeling of the initial imperfection of thin shell structures [15-18]. Finally, the axial displacement instead of the axial compressive force is applied at the edges of the isogrid-stiffened cylinder considering the geometrical initial imperfection for the postbuckling analysis since Newton-Raphson method with the displacement control method is applied with an artificial damping [23] for the present postbuckling analysis. The artificial damping with the value of 5% is used to stabilize nonlinear analysis with local instabilities such as snapthrough, local buckling, and wrinkling because it dissipates the released strain energy when a local instability occurs. In addition, all the nodes at each resin ring region of the cylinder, all the modes are coupled with a control node using rigid links (Figure 7) for a uniform displacement condition. The axial displacement instead of the axial force is applied to a control node for the displacement control method.

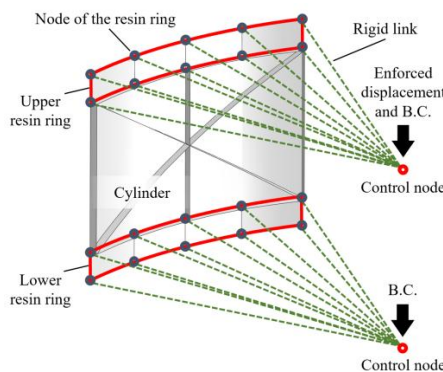


Figure 7: Rigid rinks and control nodes.

In this step, the relationship between the axial force and displacement of a cylinder under axial compressive forces is obtained along with the predicted global and local buckling loads. The process above is repeated as the single perturbation load is increased until the global buckling load converges. As shown in Figure 8, as the radial perturbation load increases, the global buckling load of a cylinder with the geometrical initial imperfection decreases as compared with that of a perfect cylinder without the initial imperfection. In the SPLA, when the perturbation load exceeds a certain perturbation load ( $Q_1$  in Figure 8) the global buckling load of a cylinder with the initial imperfection does not decrease but is almost constant although the single perturbation load increases further. The corresponding buckling load is defined as the design load ( $N_1$ ) of the cylinder for the postbuckling analysis.

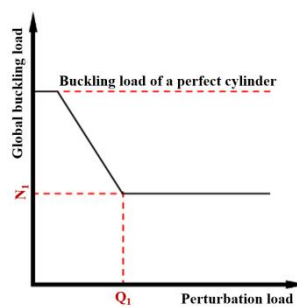


Figure 8: Global buckling load in terms of a perturbation load.

Using the calculated global buckling loads with and without the initial imperfection, the shell Knockdown factor,  $\gamma$ , is derived as

$$\gamma = \frac{(N_{cr})_{\text{imperfect}}}{(N_{cr})_{\text{perfect}}} \quad (13)$$

where  $(N_{cr})_{\text{imperfect}}$  and  $(N_{cr})_{\text{perfect}}$  are the global buckling loads of a cylinder with and without the initial imperfection, respectively.

### 3. Numerical result

#### 3.1 Shell thickness ratio of $R/t_{\text{eff}}=441$ (baseline model)

Prior to the postbuckling analyses and derivation of the Knockdown factors of the isogrid-stiffened cylinders considering various shell thickness ratios, the postbuckling analyses using both the detailed and equivalent models are conducted for the baseline model ( $R/t_{\text{eff}}=441$ , [22]) as given in Figure 4 and Table 1 and the Knockdown factors are derived using the calculated global buckling loads in this section. Figure 9 exhibits the postbuckling analyses for the baseline isogrid-stiffened cylinder model. For the perfect cylinder without the initial imperfection, the detailed and equivalent models predict the global buckling loads of 5,450 and 5,320 kN, respectively. As the perturbation load increases, the global buckling loads converge for both the detailed and equivalent models. When the initial imperfection is considered, the global buckling loads (B) are calculated as 3,290 and 3,250 kN, respectively, for the detailed and equivalent models. As given in the figure, the global buckling loads using the detailed and equivalent models are very close to each other for the isogrid-stiffened cylinders without and with the initial imperfection, since the relative errors are -2.39 and -1.22%, respectively, for global buckling loads without and with the initial imperfection. However, the predicted global buckling loads of the present both models considering the initial imperfection are different from the measured value [22] by 3.14 to 4.41%. It is believed that this discrepancy is due to the lack of detailed modeling information in Ref. [22]; however, the error is not significant, but relatively small. Figure 10 compares the deformed shapes of the baseline cylinder using the detailed and equivalent models. As seen in the figure, two models show quite similar deformed configurations of the baseline cylinder in the local buckling (A), global buckling (B), and postbuckling states (C). Using the calculated global buckling loads of the baseline model with and without the initial imperfection, the Knockdown factors are derived as 0.604 and 0.611, respectively, for the detailed and equivalent models, and they are compared well to each other. The results for postbuckling analysis and derivation of Knockdown factor for the baseline model are summarized in Table 5. As shown in Figures 9, 10, and Table 5, therefore, the present equivalent model for the isogrid-stiffened cylinder provides reasonably accurate predictions for the global buckling loads with and without the initial imperfection and the Knockdown factors in spite of using 16% of the computation time of the postbuckling analysis using the detailed model.

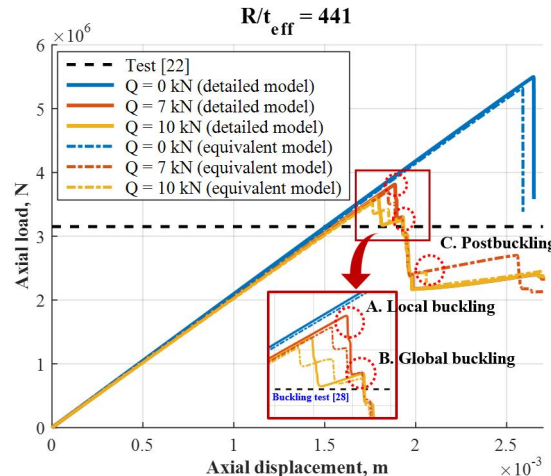


Figure 9: Postbuckling analysis results of the isogrid-stiffened cylinder ( $R/t_{\text{eff}}=441$ ).

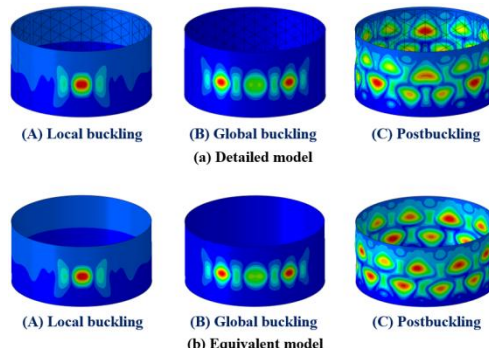


Figure 10: Deformed shapes of the isogrid-stiffened cylinder ( $R/t_{\text{eff}}=441$ ).

Table 5: Postbuckling analysis results of isogrid-stiffened cylinders with various shell thickness ratios ( $R/t_{eff}=100, 200, 300$ , and 441).

| Shell thickness ratio, $R/t_{eff}$             | 100   | 200   | 300   | 441   |
|--|-------|-------|-------|-------|
| <b>Global buckling load of perfect model</b>   |       |       |       |       |
| Detailed model, kN                             | 5,620 | 5,400 | 5,530 | 5,450 |
| Equivalent model, kN                           | 5,550 | 5,420 | 5,340 | 5,320 |
| Error, %                                       | -1.25 | 0.37  | -3.44 | -2.39 |
| <b>Global buckling load of imperfect model</b> |       |       |       |       |
| Detailed model, kN                             | 3,920 | 3,740 | 3,720 | 3,290 |
| Equivalent model, kN                           | 3,940 | 3,760 | 3,660 | 3,250 |
| Error, %                                       | 0.51  | 0.53  | -1.61 | -1.22 |
| <b>Knockdown factor</b>                        |       |       |       |       |
| Detailed model                                 | 0.698 | 0.693 | 0.673 | 0.604 |
| Equivalent model                               | 0.710 | 0.694 | 0.685 | 0.611 |
| Error, %                                       | 1.72  | 0.14  | 1.78  | 1.16  |
| <b>Computation time</b>                        |       |       |       |       |
| Detailed model, min                            | 172   | 176   | 204   | 207   |
| Equivalent model, min                          | 23    | 28    | 28    | 33    |
| Equi. model / Detailed model, (%)              | 13.4  | 15.9  | 13.7  | 15.9  |

### 3.2 Shell thickness ratio of $R/t_{eff}=300$

Using the modeling technique described in Section 2.2, the shell thickness ratio of the isogrid-stiffened cylinder is changed from the baseline value but its slenderness ratio is maintained as the baseline value. The postbuckling analysis results using the detailed and equivalent models are given in Figure 11 for the isogrid-stiffened cylinder with the shell thickness ratio of 300. For the perfect cylinder without the initial imperfection, the global buckling loads are calculated as 5,530 and 5,340 kN, respectively, using the detailed and equivalent models. These are higher than the results for the previous baseline case with  $R/t_{eff} = 441$ . When the geometrical initial imperfection is considered, the global buckling loads (B) of the isogrid-stiffened cylinder are converged to 3,720 and 3,660 kN, respectively, for the detailed and equivalent models. These global buckling loads with the initial imperfection are also higher than those of the baseline model considering the initial imperfection. The Knockdown factors are derived using Eq. (13) as 0.673 and 0.685, respectively, for the detailed and equivalent models, as given in Table 5. These Knockdown factors with  $R/t_{eff} = 300$  are higher than the results using the baseline model. As summarized in Table 5, the global buckling load and Knockdown factor predicted using the equivalent model are compared nicely well with those using the detailed model although the computation time with the equivalent model is about 14% of calculation time using the detailed model. The deformed shapes of the isogrid-stiffened cylinder in the local buckling, global buckling, and postbuckling states are plotted in Figure 12. As seen in the figure, two models give similar deformed configurations in the local buckling (A) and global buckling states (B); however, the postbuckled shapes of the cylinder (C) using the detailed and equivalent models are moderately different from each other.

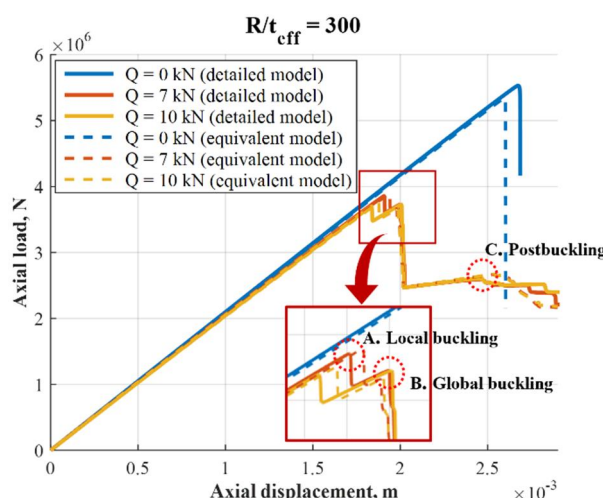
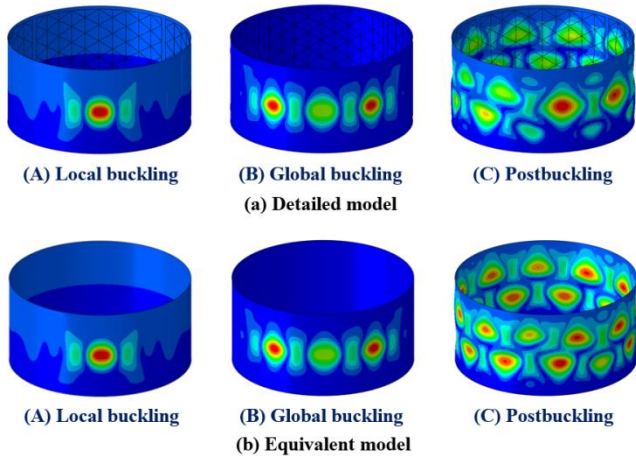
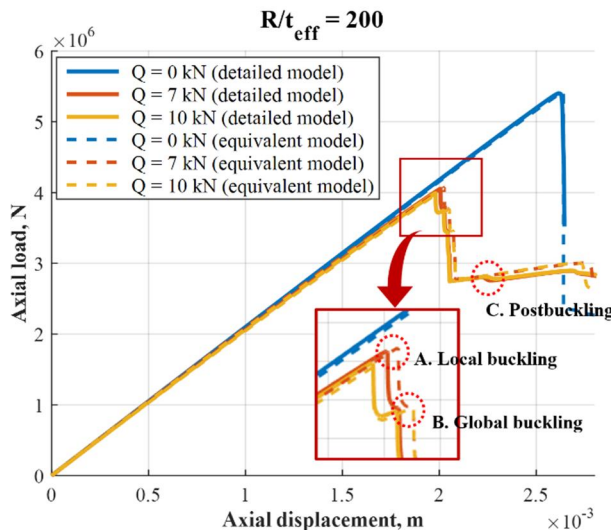


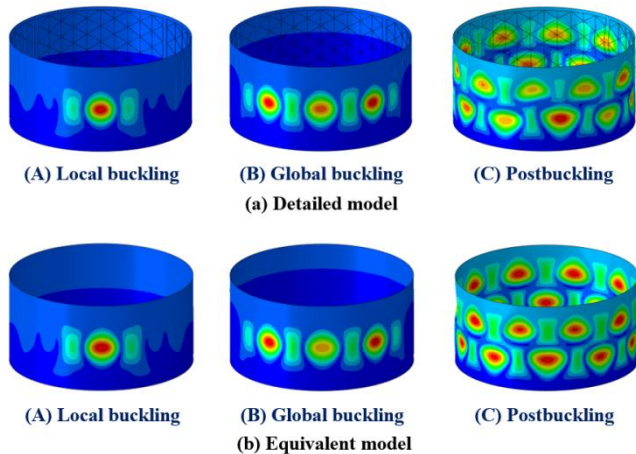
Figure 11: Postbuckling analysis results of the isogrid-stiffened ( $R/t_{eff}=300$ ).

Figure 12: Deformed shapes of the isogrid-stiffened cylinder ( $R/t_{eff}=300$ ).

### 3.3 Shell thickness ratio of $R/t_{eff}=200$

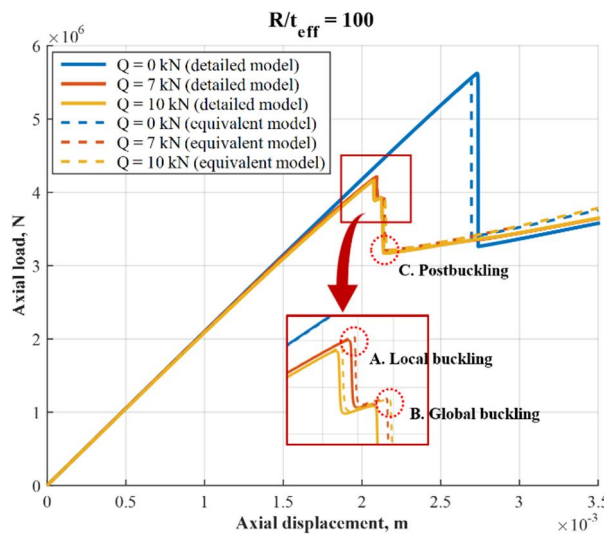
Figure 13 gives the relationship between the axial load and axial displacement in postbuckling analyses for the isogrid-stiffened cylinder with the shell thickness ratio of 200. The global buckling loads are predicted as 5,400 and 5,420 kN, respectively when the geometrical initial imperfection is not considered for the detailed and equivalent models. Two results are quite similar to each other with the relative error of 0.37%. The converged global buckling loads using the detailed and equivalent models are 3,740 and 3,760 kN, respectively, when the geometrical initial imperfection is considered. These loads are higher than the results in the previous case with  $R/t_{eff} = 300$ , and the relative error between two results using the detailed and equivalent models is 0.53% as given in Table 5. The Knockdown factors for the isogrid-stiffened cylinder with  $R/t_{eff} = 200$  are derived as 0.693 and 0.694, respectively, for the detailed and equivalent models in Table 5, thus the relative error between two results is very small (0.14%). These Knockdown factors are higher than those with  $R/t_{eff} = 300$ . As similar to the previous example, the computation time using the equivalent model is approximately 16% of that with the detailed model. Figure 14 shows the deformed shapes of the isogrid-stiffened cylinder with the shell thickness ratio of 200. As given in the figure, the deformed configurations of the cylinder in the local buckling (A), global buckling (B), and postbuckling states (C) predicted by the equivalent model are quite similar to those using the detailed model.

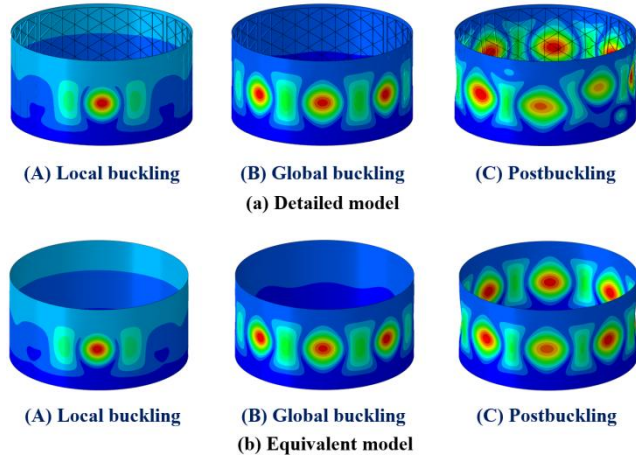
Figure 13: Postbuckling analysis results of the isogrid-stiffened cylinder ( $R/t_{eff}=200$ ).

Figure 14: Deformed shapes of the isogrid-stiffened cylinder ( $R/t_{eff}=200$ ).

### 3.4 Shell thickness ratio of $R/t_{eff}=100$

Figure 15 shows the postbuckling analyses using the detailed and equivalent models for the isogrid-stiffened cylinder with the shell thickness ratio of 100. For the perfect cylinder without the initial imperfection, the global buckling loads are calculated as 5,620 and 5,550 kN, respectively, using the detailed and equivalent models. For the cylinder considering the initial imperfection, the global buckling loads predicted by the detailed and equivalent models both are converged well as the perturbation load increases. The detailed and equivalent models predict the global buckling loads (B) as 3,920 and 3,940 kN, respectively for the isogrid-stiffened cylinder with the initial imperfection. The relative errors for the cylinder without and with the initial imperfection are given as -1.25 and 0.51%, respectively, as summarized in Table 5. In addition, the global buckling loads of the isogrid-stiffened cylinder with  $R/t_{eff}=100$  are higher than those with  $R/t_{eff}=200$  in the previous example. Using the calculated global buckling loads with and without the initial imperfection, the Knockdown factors are derived as 0.698 and 0.710, respectively, for the detailed and equivalent models. As similar to the previous case, the derived Knockdown factors using two models are similar to each other and they are higher than the Knockdown factors with  $R/t_{eff}=200$ . As given in Table 5, the calculation time using the equivalent model is about 13% of that with the detailed model although the global buckling load and Knockdown factor predicted using the equivalent model are compared nicely with those using the detailed model. The deformed shapes of the isogrid-stiffened cylinder with  $R/t_{eff}=100$  are plotted in Figure 16. In the local buckling (A), global buckling (B), and postbuckling states (C), the detailed and equivalent models show the similar deformed configurations to each other.

Figure 15: Postbuckling analysis results of the isogrid-stiffened cylinder ( $R/t_{eff}=100$ ).

Figure 16: Deformed shapes of the isogrid-stiffened cylinder ( $R/t_{\text{eff}}=100$ ).

### 3.5 Knockdown factor function in terms of shell thickness ratio

The Knockdown factor should be expressed in terms of the shell thickness ratio for lightweight design of isogrid-stiffened cylinders considering various dimensions. Similarly to the NASA's Knockdown factor function [1] given by Eq. (14), the Knockdown factor function for the isogrid-stiffened cylinder is derived using the calculated Knockdown factors in the previous sections. Using the curve fitting, the present Knockdown factor function is derived based on the form of NASA's Knockdown factor function shown in Eq. (14). The curve-fitting tool with the exponential model in MATLAB [24] is used for the curve fitting in this study. Equations (15) and (16) represent the Knockdown factor functions of the isogrid-stiffened cylinder using the detailed and equivalent models, respectively.

$$\gamma = 1 - 0.902(1 - e^{-\frac{1}{16}\sqrt{\frac{R}{t_{\text{eff}}}}}) \quad (14)$$

Using the detailed model,

$$\gamma = 1 - 0.5386(1 - e^{-\frac{1}{16}\sqrt{\frac{R}{t_{\text{eff}}}}}) \quad (15)$$

Using the equivalent model,

$$\gamma = 1 - 0.5256(1 - e^{-\frac{1}{16}\sqrt{\frac{R}{t_{\text{eff}}}}}) \quad (16)$$

Figure 17 compares the Knockdown factor functions for the isogrid-stiffened cylinder derived in this work with the NASA's Knockdown factor function. As shown in this figure, the calculated Knockdown factors using the detailed and equivalent models are quite similar to each other when the shell thickness ratios are 100, 200, 300, and 441. In addition, the present Knockdown factor values using the detailed and equivalent models both are compared excellently with the value given in the reference [22] when the shell thickness ratio is 441. Thus, the Knockdown factors derived using two models are validated successfully in this paper. When the present Knockdown factor functions using the detailed and equivalent models (Eqs. (15) and (16)) are nearly identical when the shell thickness ratio is up to 500. Furthermore, the Knockdown factor functions in the present work are much higher than NASA's Knockdown factor function; therefore, the buckling design of isogrid-stiffened cylinders using the present Knockdown factor function can facilitate in developing lightweight launch vehicle structures as compared with the design using the previous buckling design criteria [1].

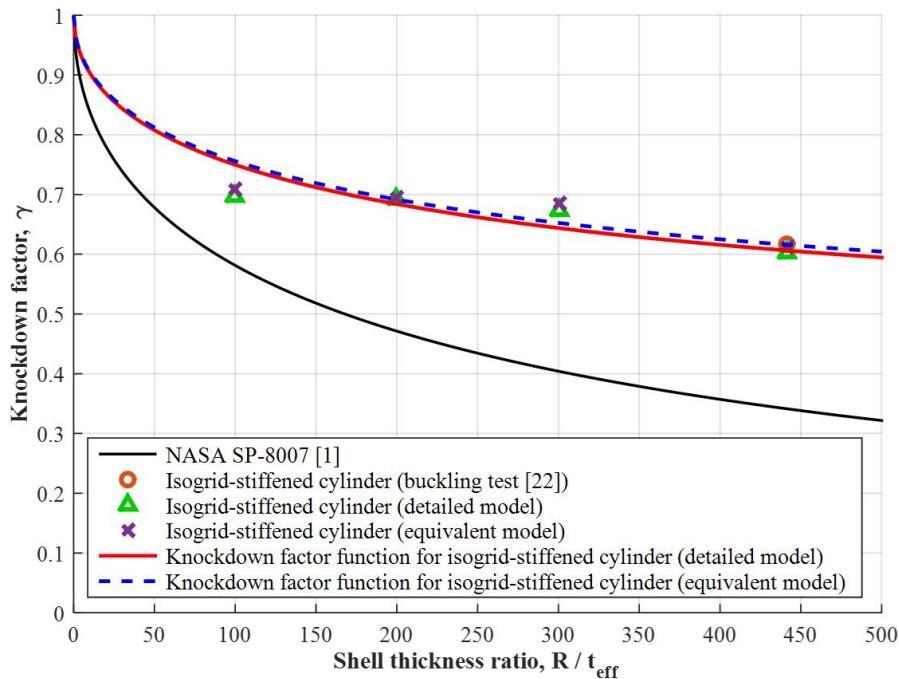


Figure 17: Knockdown factor function for the isogrid-stiffened cylinder in terms of the shell thickness ratio.

#### 4. Conclusion

This study derived numerically the buckling Knockdown factors of isogrid-stiffened cylinders under axial compressive loads when various shell thickness ratios were considered. The isogrid-stiffened cylinders with shell thickness ratios of 100, 200, 300, and 441 were used. The detailed model considering numerous stiffeners and the equivalent model without modeling of stiffeners were used for the finite element modeling of isogrid-stiffened cylinders. Postbuckling analyses using ABAQUS were conducted for the isogrid-stiffened cylinders represented by the detailed and equivalent models to derive the Knockdown factors. The geometrical initial imperfection of a cylinder was modeled using the SPLA and Newton-Raphson method with the displacement control method was applied for the nonlinear static postbuckling analyses. For all the shell thickness ratios considered in this study, the global buckling loads using the equivalent model were quite similar to the results with the detailed model since the relative errors were within 5% for the cylinders with and without the initial imperfection. In addition, the derived Knockdown factors with the equivalent model were compared excellently with the values using the detailed model because the relative errors were less than 2%. In addition to these accurate prediction capability of the equivalent model for isogrid-stiffened cylinders, since the computation time with the equivalent model was 13 to 16% of that using the detailed model, the equivalent modeling technique was very efficient for the finite element modeling and postbuckling analysis of isogrid-stiffened cylinders under compressive axial forces. Using the calculated Knockdown factors, the Knockdown factor functions for isogrid-stiffened cylinders were expressed in terms of the shell thickness ratio. Knockdown factor functions using the detailed and equivalent models were quite similar to each other. Furthermore, the present Knockdown factor function for the isogrid-stiffened cylinder was much higher than NASA's Knockdown factor function when the shell thickness ratio of up to 500 was considered; therefore, it was concluded that the present Knockdown factor function can facilitate in developing lightweight launch vehicle structures using the isogrid-stiffened cylinder.

#### Acknowledgment

This work was supported by research on the preceding technologies for geostationary satellite launch vehicle of the Korea Aerospace Research Institute (KARI). This work was supported by the Korea Launch Vehicle (KSLV-II) funded by the Ministry of Science and ICT (MSIT, Korea).

## References

- [1] Weingarten, V.I., Seide, P., and Peterson, J.P. 1968. Buckling of thin-walled circular cylinders. NASA SP-8007.
- [2] Hilburger, M.W. 2018. On the development of shell buckling Knockdown factors for stiffened metallic launch vehicle cylinders. In: *AIAA/ASME/ASCE/AHS/ASC Structures, Structural Dynamics and Materials Conference, Structures, Structural Dynamics, and Materials and Co-located Conferences*.
- [3] Khakimova, R., Zimmermann, R., Wilckens, D., Rohwer, K., and Degenhardt, R. 2016. Buckling of axially compressed CFRP truncated cones with additional lateral load: Experimental and numerical investigation. *Composite Structures*, 157:436-447.
- [4] Hilburger, M.W. 2012. Developing the next generation shell buckling design factors and technologies. In: *AIAA/ASME/ASCE/AHS/ASC Structures, Structural Dynamics and Materials Conference, Structures, Structural Dynamics, and Materials and Co-located Conferences*.
- [5] Hilburger, M.W., Lovejoy, A., Thorneburgh, R., and Rankin, C. 2012. Design and analysis of subscale and full-scale buckling-critical cylinders for launch vehicle technology development. In: *AIAA/ASME/ ASCE/AHS/ASC Structures, Structural Dynamics and Materials Conference, Structures, Structural Dynamics, and Materials and Co-located Conferences*.
- [6] Hilburger, M.W., Waters, W.A., and Hynie, W.T. 2015. Buckling test results from the 8-foot-diameter orthogrid-stiffened cylinder test article TA01. NASA TP-2015-218785.
- [7] Degenhardt, R., Kling, A., Zimmermann, R., Odermann, F., Araújo, F.C.D. 2012. Dealing with imperfection sensitivity of composite structures prone to buckling. *Advances in computational stability analysis*.
- [8] Khakimova, R., Charistopher, J.W., Zimmermann, R., Castro, S.G.P., Arbelo, M.A., and Degenhardt, R. 2014. The single perturbation load approach applied to imperfection sensitive conical composite structures. *Thin-Walled Structures*. 84:369-377.
- [9] Di Pasqua, M.F., Khakimova, R., Castro, S.G.P., Arbelo, M.A., Riccio, A., and Degenhardt, R. 2015. The influence of geometrical parameters on the buckling behavior of conical shell by the single perturbation load approach. *Applied Composite Materials*. 22:405-422.
- [10] Wagner, H.N.R., Hühne, C., Niemann, S. 2017. Robust knockdown factors for the design of axially loaded cylindrical and conical composite shells development and validation. *Composite Structures*. 173:281-303.
- [11] Wang, B., Hao, P., Li, G., Zhang, J.X., Du, K.F., Tian, K., and Tang, X.H. 2014. Optimum design of hierarchical stiffened shells for low imperfection sensitivity. *Acta Mechanica Sinica*. 30:391-402.
- [12] Meyer, R.R., Harwood, O.P., Harmon, M.B., and Orlando J.I. 1973. Isogrid design handbook. NASA CR-124075.
- [13] Yoo, J.-T., Jang, Y.-S., and Yi Y.-M. 2005. Structural design and development of isogrid cylinder for propellant tank. In: *56<sup>th</sup> Astronautical Congress of the International Astronautical Federation, the International Academy of Astronautics, and the International Institute of Space Law*.
- [14] Tian, K., Wang, B., Hao, P., and Antony M.W. 2018. A high-fidelity approximate model for determining lower bound buckling load for stiffened shells. *International Journal of Solids and Structures*. 148-149:14-23.
- [15] Castro, S.G.P., Zimmermann, R., Arbelo, M.A., and Degenhardt, R. 2013. Exploring the constancy of the global buckling load after a critical geometric imperfection level in thin-walled cylindrical shells for less conservative knock-down factors. *Thin-Walled Structures*. 72:76-87.
- [16] Deml, M., and Wunderlich, W. 1997. Direct evaluation of the worst imperfection shape in shell buckling. *Computer Methods in Applied Mechanics and Engineering*. 149:201-222.
- [17] Haynie, W., Hilburger, M.W., Bogge, M., Maspoli, M., and Kriegesmann, B. 2012. Validation of lower-bound estimates for compression-loaded cylindrical shells. In: *14<sup>th</sup> AIAA/ASME/ASCE/AHS/ASC Structures, Structural Dynamics and Materials and Co-located Conferences*.
- [18] Castro, S.G.P., Zimmermann, R., Arbelo, M.A., Khakimova, R., Hilburger, M.W., and Degenhardt, R. 2014. Geometric imperfections and lower-bound methods used to calculate knock-down factors for axially compressed composite cylindrical shells. *Thin-Walled Structures*. 74:118-132.
- [19] Sim, C.-H., Kim, H.-I., Lee, Y.-L., Park, J.-S., and Lee, K.J. 2018. Postbuckling analyses and derivations of Knockdown factors for hybrid-grid stiffened cylinders. *Aerospace Science and Technology*. 82:20-31.

- [20] Sim, C.-H., Kim, H.-I., Lee, Y.-L., Park, J.-S., and Lee, K.J. 2018. Derivations of knockdown factors for cylindrical structures considering different initial imperfection models and thickness ratios. *International Journal of Aeronautical and Space Sciences*. 19:626-635.
- [21] Hühne, C., Rilfes, R., Breitbach, E., and Temer, J. 2008. Robust design of composite cylindrical shells under axial compression-simulation and validation. *Thin-Walled Structures*. 46:947-962.
- [22] Wang, B., Du, K., Hao, P., Zhou, C., Tian, K., Xu, S., Ma, Y., and Zhang, X. 2016. Numerical and experimentally predicted knockdown factors for stiffened shells under axial compression. *Thin-Walled Structures*. 109:13-24.
- [23] White, S.C., Weaver, P.M., and Wu, K.C. 2015. Post-buckling analyses of variable-stiffness composite cylinders in axial compression. *Composite Structures*. 123:190-203.
- [24] MATLAB *Curve fitting toolbox: User's guide*. <https://www.mathworks.com/help/curvefit/exponential.html>.